

X-ray and Raman scattering measurements in finite, pseudomorphically strained, Fibonacci lattices

A. T. Macrander, G. P. Schwartz, and J. Bevk

AT&T Bell Laboratories, Murray Hill, New Jersey 07974-2070

(Received 11 January 1988)

X-ray and Raman scattering measurements have been performed on pseudomorphically strained $\text{Si}/\text{Ge}_x\text{Si}_{1-x}$ Fibonacci lattices with low stage numbers. Both the x-ray and Raman measurements exhibit significant deviations from large-stage behavior for Fibonacci lattices with fewer than ten stages. A kinematical expression for the diffracted x-ray intensity of a strained-layer Fibonacci lattice is derived in the limit of large stage number.

Recent reports by Merlin *et al.*^{1,2} and Dharmawardana and co-workers³ have demonstrated that pseudo-one-dimensional Fibonacci lattices exhibit properties that are uniquely associated with their quasiperiodic structure. The electronic and vibrational eigenfrequency spectra of the Fibonacci lattice have received considerable theoretical attention,⁴⁻⁸ particularly in the limit of large stage number where the system simulates the properties of a lattice of nearly infinite extent. It is in the low-stage-number regime, however, where the eigenfrequency spectrum becomes sparse, that one can explicitly study the shifts in eigenfrequencies with changing stage number. In this paper we report the first x-ray and Raman scattering measurements on pseudomorphically strained Fibonacci lattices grown with exceptionally low-order stage numbers.

The prescription for forming a Fibonacci lattice from two structural units A and B can be found in the literature.¹ Designating H_A and H_B as the number of A and B units for a given stage N , our tenth-, eighth-, and sixth-stage samples consist of 89, 34, and 13 total layers distributed according to (H_A, H_B) pairs of (55,34), (21,13), and (8,5) respectively. The Fibonacci lattices were grown on (100) Si substrate using molecular-beam epitaxy with nominal A ($\text{Si}_{0.8}\text{Ge}_{0.2}$) and B (Si) layer widths d_A and d_B of 44.4 and 27.2 Å. For this alloy composition, the lattice mismatch is $\sim 0.84\%$. In order to ensure that the A and B layer deposition rates were equivalent for all stages, the samples were grown on a single substrate during one run with a shutter which could be translated along the substrate. Experimental details were published previously.⁹

Figure 1 displays experimental and simulated x-ray rocking curves for the (400) reflection from our Fibonacci lattices. The experimental data for the stage-10 sample (nominal thickness 3441 Å) exhibited line broadening indicative of misfit dislocations and are not shown.⁹ The dynamical simulation incorporated absorption and was made using Abeles' method,^{10,11} assuming pseudomorphic epitaxy. Refined x-ray parameters were used for d_A and d_B (44.0 and 29.9 Å, respectively) in the simulation and a tetragonal distortion of the alloy layers was included.¹² The arrows and solid symbols represent the peak

positions and intensities calculated using kinematical theory including strain for a Fibonacci lattice of infinite extent.

Since strain has not been incorporated in previous treatments of x-ray rocking curves of Fibonacci lattices, we present a short derivation of the necessary kinematical theory in the following text. Comparison of the kine-

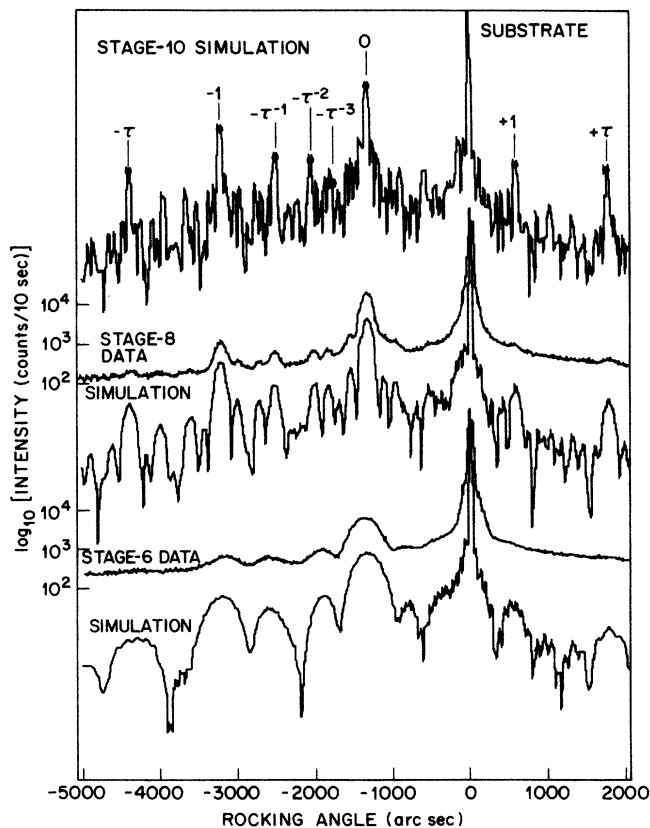


FIG. 1. Simulated and measured x-ray rocking curves of the (400) reflection for stage-6, -8, and -10 Fibonacci lattices. The arrows and solid circles in the top panel indicate the peak positions and intensities for a Fibonacci lattice of infinite extent calculated using the kinematical theory derived in the text. The kinematical peaks are labeled according to $m\tau + n$ notation.

matic and simulated x-ray rocking curves for the stage-10 Fibonacci lattice already demonstrates that many properties of quasiperiodic structures will be nearly independent of sample length (volume) for quite finite systems. As the stage number is reduced, however, sample size effects begin to manifest in a fashion which is not merely a broadening of higher stage spectra.

In order to incorporate strain in a kinematical theory for x-ray diffraction from a Fibonacci lattice, one starts analogously to the periodic lattice case by expressing the angular deviation $\Delta\omega_j$ of the rocking angle θ_r for the j th layer in terms of the Bragg angle of the substrate θ_B^s and the j th layer lattice mismatch $(\Delta a/a)_j$ as $\Delta\omega_j = (\theta_r - \theta_B^s) + (\Delta a/a)_j \tan\theta_B^s$. It is readily shown that to first order in $\Delta\omega_j$ and $(\Delta a/a)_j$, $k \equiv 2\pi(2\sin\theta_r)/\lambda = 2\pi h/a_j + 2\alpha_j/a_j$ for an $(h00)$ reflection. In this expression $\alpha_j = \pi h(\cot\theta_B^s)\Delta\omega_j$, and λ is the x-ray wavelength. Standard expressions for the diffracted electric field amplitude¹³ then yield

$$E = F_A \exp(i\alpha_A N_A) \frac{\sin[\alpha_A(N_A + 1)]}{\sin\alpha_A} \times \sum_{\{j\}_A} \exp\left[2i \sum_{l=0}^{j-1} \alpha_l N_l\right] + F_B \exp(i\alpha_B N_B) \frac{\sin[\alpha_B(N_B + 1)]}{\sin\alpha_B} \times \sum_{\{j\}_B} \exp\left[2i \sum_{l=0}^{j-1} \alpha_l N_l\right]. \quad (1)$$

Here N_j is the number of unit cells in the j th layer, F_j is the usual x-ray structure factor, and j values start with 1 for the first Fibonacci lattice layer grown ($\alpha_0 \equiv 0$). The sums are restricted to j values at either an A or B layer. In order to evaluate the sums we utilize the concepts outlined in Ref. 3 and invoke a two-dimensional periodic hyperspace with spacings given by $a_x = \alpha_A N_A (1 + 1/\gamma\tau)^{1/2}$ and $a_y = \alpha_B N_B (1 + \gamma\tau)^{1/2}$ where $\gamma \equiv \alpha_A N_A / \alpha_B N_B$ and $\tau = (1 + \sqrt{5})/2$. If this space is cut by an axis ξ at an angle ϕ satisfying $\cot\phi = \tau a_x / a_y$, and hyperspace lattice points within a band W of width $a_x \sin\phi + a_y \cos\phi$ around this line are projected onto ξ , a Fibonacci sequence in $\alpha_A N_A$ and $\alpha_B N_B$ results. Denoting $\xi = \bar{m}a_x \cos\phi + \bar{n}a_y \sin\phi$ as the (\bar{m}, \bar{n}) coordinate of a lattice point in the hyperspace, sums of the form $\sum_{\{j\}_A} \exp(2i \sum_{l=0}^{j-1} \alpha_l N_l)$ are converted to $\sum_{(\bar{m}, \bar{n})_A} \exp(2i\bar{\xi})$ and similarly for the $\{j\}_B$ sums. By performing the Fibonacci lattice inflation $A' = AB$ and $B' = A$ once for an A layer sum and twice for a B layer sum, the restricted sums in Eq. (1) entailing (\bar{m}, \bar{n}) points only for A layers can be converted to unrestricted sums over new indices (\bar{m}', \bar{n}') . By projecting all the points in the band onto the hyperspace axis perpendicular to ξ , we can convert the sums to integrals for a Fibonacci lattice of infinite extent, since in this case the density of projected points can be taken to be uniform.¹⁴ The results for the A and B sums yield

$$\sum_{(\bar{m}, \bar{n})_A} \exp(2i\bar{\xi}) = M_A \exp(iZ\tau) \frac{\sin(Z/\tau)}{(Z/\tau)} \delta(1 - \xi), \quad (2a)$$

$$\sum_{(\bar{m}, \bar{n})_B} \exp(2i\bar{\xi}) = M_B \exp(-iZ/\tau^2) \exp(2i\alpha_A N_A) \times \frac{\sin(Z/\tau^2)}{(Z/\tau^2)} \delta(1 - \xi), \quad (2b)$$

where M_A and M_B measure the number of points of type A or B within the strip W . Here ξ is the (m, n) reciprocal space coordinate given by $(m \cos\phi/a_x + n \sin\phi/a_y)\pi$, and Z is given by $\pi\tau(n\gamma - m)/(\gamma + 1/\tau)$. The δ -function condition can be rewritten as $1 = \pi(m\tau + n)/(\tau\alpha_A N_A + \alpha_B N_B)$, which for the (400) reflection yields $k = 8\pi/\langle a \rangle + (2\pi/d)(m\tau + n)$, with $d = \tau\alpha_A N_A + \alpha_B N_B$ and $\langle a \rangle = d/(\tau N_A + N_B)$, which represent the period and average lattice parameter of the Fibonacci lattice. Substituting Eqs. (2a) and (2b) back into Eq. (1) and noting that $\alpha_A N_A = m\pi + Z/\tau^2$ and $\alpha_B N_B = n\pi - Z/\tau$, we obtain for the diffracted electric field amplitude

$$E_{m,n} = \frac{M_A \tau}{Z} \sin\left[\frac{Z}{\tau}\right] \sin\left[\frac{Z}{\tau^2}\right] \times \left[\frac{F_A}{\sin(\alpha_A)} - \frac{F_B}{\sin(\alpha_B)} \right] \delta(1 - \xi), \quad (3)$$

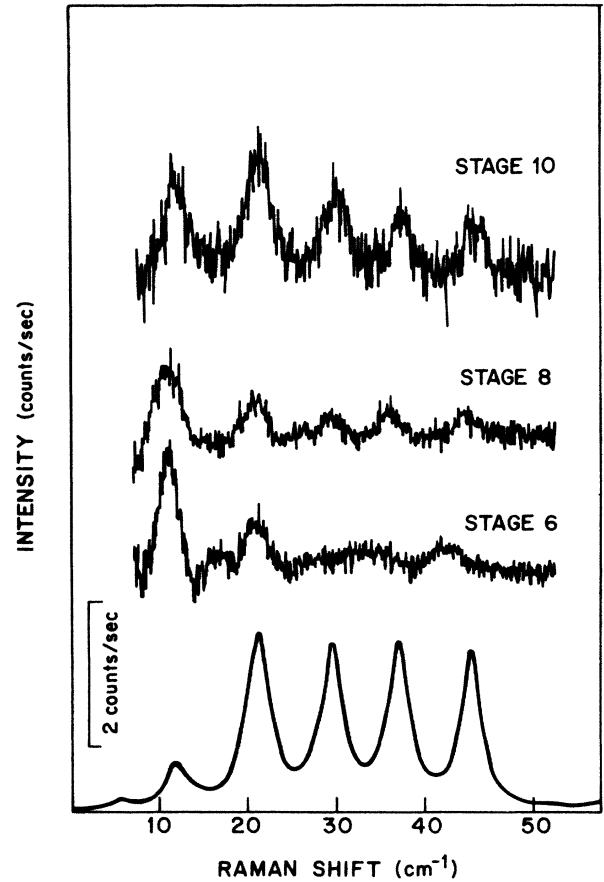


FIG. 2. Polarized Raman spectra for stage-10, -8, and -6 Fibonacci lattices taken with 5145-Å excitation. The instrumental resolution was 2.5 cm^{-1} , and the Rayleigh wing has been removed from the data. The bottom panel represents a simulation of the Raman spectrum of a large-stage Fibonacci lattice with layer parameters equal to those of our samples.

where we have used the fact that for an infinite Fibonacci lattice $M_A = \tau M_B$.

Equation (3) predicts that in a pseudomorphically strained Fibonacci lattice, the x-ray intensity E^2 should be modulated by both structure factor and strain terms. In the strain-free case the intensities are symmetric around the average lattice peak ($m = n = 0$), whereas in a strained Fibonacci lattice the peak amplitudes are asymmetric, as shown in Fig. 1. The excellent agreement between the kinematic model (scaled to the average lattice peak intensity) and the tenth-stage Abeles' simulation provides an indicator of the finite length scale necessary to approximate a lattice of infinite extent.

Figure 2 shows polarized $z(x', x')\bar{z}$ Raman spectra [$z = (001)$, $x' = (110)$] of the symmetry-allowed longitudinal-acoustic phonons propagating parallel to the (001) axis in stage-6, -8, and -10 Fibonacci lattices. Numerical analysis of the acoustic eigenfrequencies of a one-dimensional Fibonacci chain has shown that in the long-wavelength regime the number of gaps and their size tends to zero as the chain length is increased.⁴ Thus in the large stage limit the acoustic modes of a Fibonacci lattice will resemble zone folded modes in a periodic structure, and the observed frequencies can be approximated by $\omega_{m,n} = |\omega_0(m\tau + n) \pm \omega_B|$, where $\omega_0 \equiv 2\pi V_{FL} / (d_B + \tau d_A)$, V_{FL} is the average acoustic velocity in the Fibonacci lattice, and ω_B is the Brillouin frequency.³ The intensity modulation of these peaks has been derived in Ref. 3 in the same limit of large stage number for arbitrary values of d_A and d_B .

Pseudomorphic epitaxy will result in a small tetragonal distortion of the $\text{Si}_x\text{Ge}_{1-x}$ layer width, but the effect on the intensity modulation pattern is negligible. Similarly,

any strain-induced changes in the photoelastic coefficients only serve to rescale the overall intensity pattern. Since ω_0 and ω_B are empirically determined from the data, the simulated Raman spectrum already contains the effects of strain.

The bottom panel of Fig. 2 represents a simulation of the tenth-stage Raman spectrum using 30 selected (m, n) pairs chosen to yield peaks in the range $\omega_{m,n} < 60 \text{ cm}^{-1}$ which are modulated in intensity according to Ref. 3. The simulation parameters were $\omega_0 = 25.57 \text{ cm}^{-1}$, $\omega_B = 4.11 \text{ cm}^{-1}$, $d_A = 44.0 \text{ \AA}$, $d_B = 29.9 \text{ \AA}$, and $V_{FL} = 7.75 \times 10^5 \text{ cm/sec}$, and the peaks were Lorentzian broadened in order to compare with the data. The comparison with the stage-10 data is quite reasonable except for the intensity of the lowest-frequency peaks, which are quite sensitive to the functional line shape used to remove the Rayleigh wing. The four most intense $\omega_{m,n}$ peaks identified in the simulation are those for which $m\tau + n = 1$ and τ . The spectral redistribution accompanying stage reduction cannot be simply described by a uniform peak shift coupled with line broadening as has been recently observed in periodic superlattices.¹⁵ The shift in phonon eigenfrequencies and the redistribution of gaps at very low stage numbers is a unique aspect of quasiperiodic lattices which are seen in phonon calculations for finite Fibonacci chains.⁵ These measurements represent the first experimental verification of shifts in the phonon eigenfrequencies in the regime of exceptionally low stage numbers.

We would like to thank J. P. Mannaerts for his expert technical assistance.

- ¹R. Merlin, K. Bajema, F.-Y. Juang, and P. K. Bhattacharya, *Phys. Rev. Lett.* **55**, 1768 (1985).
²J. Todd, R. Merlin, Roy Clarke, K. M. Mohanty, and J. D. Axe, *Phys. Rev. Lett.* **57**, 1157 (1986).
³M. W. C. Dharma-wardana, A. H. MacDonald, D. J. Lockwood, J. M. Baribeau, and D. C. Houghton, *Phys. Rev. Lett.* **58**, 1761 (1987).
⁴J. P. Lu, T. Odagaki, and J. L. Birman, *Phys. Rev. B* **33**, 4809 (1986).
⁵M. Kohmoto and J. R. Banavar, *Phys. Rev. B* **34**, 563 (1986).
⁶M. Fujita and K. Machida, *Solid State Commun.* **59**, 61 (1986).
⁷F. Nori and J. P. Rodriguez, *Phys. Rev. B* **34**, 2207 (1986).

- ⁸Y. Liu and R. Riklund, *Phys. Rev. B* **35**, 6034 (1987).
⁹J. Bevk, J. P. Mannaerts, L. C. Feldman, B. A. Davidson, and A. Ourmazd, *Appl. Phys. Lett.* **49**, 286 (1986).
¹⁰D. W. Berreman, *Phys. Rev. B* **14**, 4313 (1976).
¹¹A. T. Macrander, E. R. Minami, and D. W. Berreman, *J. Appl. Phys.* **60**, 1364 (1986).
¹²J. Hornstra and W. J. Bartels, *J. Cryst. Growth* **44**, 513 (1978).
¹³B. E. Warren, *X-Ray Diffraction* (Addison-Wesley, Reading, Mass., 1969), p. 28.
¹⁴V. Elser, *Acta Crystallogr., Sect. A* **412**, 36 (1986).
¹⁵M. Nakayama, K. Kubota, H. Kato, and N. Sano, *J. Appl. Phys.* **60**, 3289 (1986).